High Harmonic Generation in Molecules, II

Chris Greene

Dept. of Physics and JILA

University of Colorado (chris.greene @ colorado.edu)

Support

Dept. of Energy, Basic Energy Sciences, Office of Science

+NSF EUV-ERC

Zach Walters

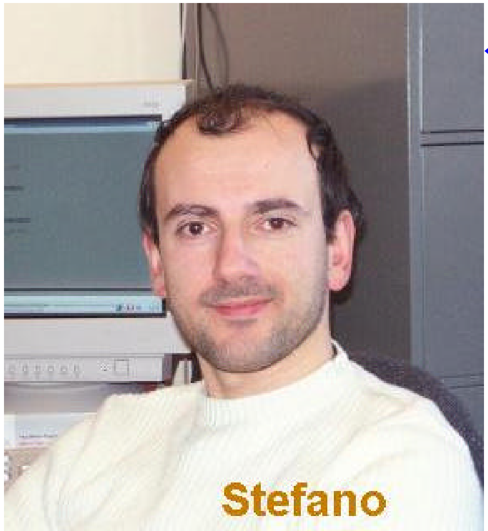

Stefano Tonzani

Collaborators on the *theoretical* projects discussed in this talk

Cautionary comments concerning recent attempts to reconstruct the "images" of molecular orbitals, using high-harmonic generation *(this analysis is based on a preliminary study, in collaboration with Stefano Tonzani and Zach Walters)*

NATURE | VOL 432 | 16 DECEMBER 2004 | www.nature.com/nature

articles

Tomographic imaging of molecular orbitals

J. Itatani[1,2], J. Levesque[1,3], D. Zeidler[1], Hiromichi Niikura[1,4], H. Pépin[3], J. C. Kieffer[3], P. B. Corkum[1] & D. M. Villeneuve[1]

[1]*National Research Council of Canada, 100 Sussex Drive, Ottawa, Ontario K1A 0R6, Canada*
[2]*University of Ottawa, 150 Louis Pasteur, Ottawa, Ontario K1N 6N5, Canada*
[3]*INRS- Energie et Materiaux, 1650 boulevard Lionel-Boulet, CP 1020, Varennes, Québec J3X 1S2, Canada*
[4]*PRESTO, Japan Science and Technology Agency, 4-1-8 Honcho Kawaguchi Saitama, 332-0012, Japan*

Single-electron wavefunctions, or orbitals, are the mathematical constructs used to describe the multi-electron wavefunction of molecules. Because the highest-lying orbitals are responsible for chemical properties, they are of particular interest. To observe these orbitals change as bonds are formed and broken is to observe the essence of chemistry. Yet single orbitals are difficult to observe experimentally, and until now, this has been impossible on the timescale of chemical reactions. Here we demonstrate that the full three-dimensional structure of a single orbital can be imaged by a seemingly unlikely technique, using high harmonics generated from intense femtosecond laser pulses focused on aligned molecules. Applying this approach to a series of molecular alignments, we accomplish a tomographic reconstruction of the highest occupied molecular orbital of N_2. The method also allows us to follow the attosecond dynamics of an electron wave packet.

From Itatani et al, Nature 2004:

Tomographic imaging of a molecular orbital is achieved in three crucial steps. (1) Alignment of the molecular axis in the laboratory frame. (2) Selective ionization of the orbital. (3) Projection of the state onto a coherent set of plane waves.

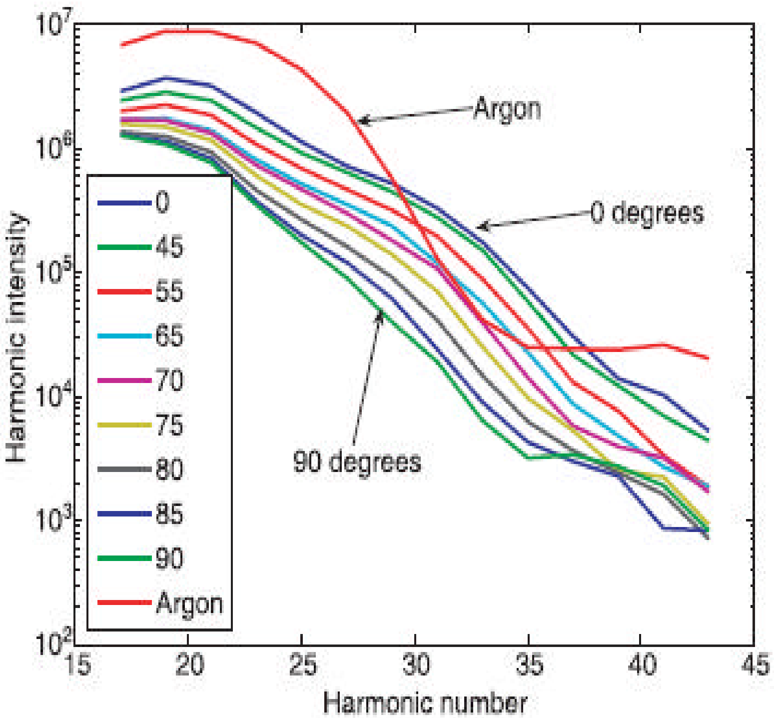

Figure 3 High harmonic spectra were recorded for N_2 molecules aligned at 19 different angles between 0 and 90° relative to the polarization axis of the laser. For clarity, only some of the angles have been plotted above. The high harmonic spectrum from argon is also shown; argon is used as the reference atom. Clearly the spectra depend on both the alignment angle and shape of the molecular orbital.

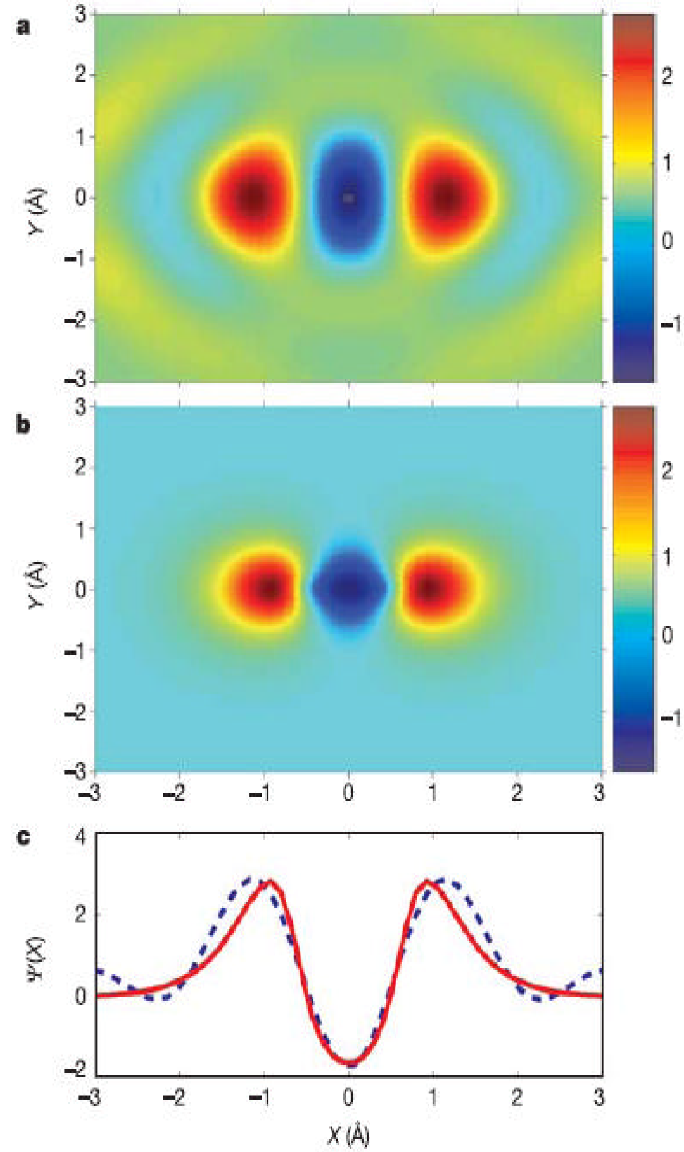

Figure 4 Molecular orbital wavefunction of N_2. **a**, Reconstructed wavefunction of the HOMO of N_2. The reconstruction is from a tomographic inversion of the high harmonic spectra taken at 19 projection angles. Both positive and negative values are present, so this is a wavefunction, not the square of the wavefunction, up to an arbitrary phase. **b**, The shape of the N_2 $2p\,\sigma_g$ orbital from an *ab initio* calculation. The colour scales are the same for both images. **c**, Cuts along the internuclear axis for the reconstructed (dashed) and *ab initio* (solid) wavefunctions.

A 2006 PRL by Santra and Gordon, which discusses some issues about the tomographic reconstruction of orbitals, and stresses that there is a minimal difference between Dyson and Hartree-Fock orbitals, in this context:

Three-Step Model for High-Harmonic Generation in Many-Electron Systems

Robin Santra

Argonne National Laboratory, Argonne, IL 60439, USA

Ariel Gordon

Research Laboratory of Electronics, Massachusetts Institute of Technology, 77 Massachusetts Ave., Cambridge, MA 02139, USA

(Dated: January 23, 2006)

The three-step model (TSM) of high-harmonic generation (HHG) is generalized to atomic and molecular many-electron systems. Using many-body perturbation theory, corrections to the standard TSM due to exchange and electron–electron correlations are derived. It is shown that canonical Hartree-Fock orbitals represent the most appropriate set of one-electron states for calculating the HHG spectrum. To zeroth order in many-body perturbation theory, a HHG experiment allows direct access in general to a combination of occupied Hartree-Fock orbitals rather than to the highest occupied molecular orbital by itself.

Example of the atomic S wavefunctions at 1 a.u. (27.2 eV) for a free particle, for a hydrogen electron, and for a "neon electron"

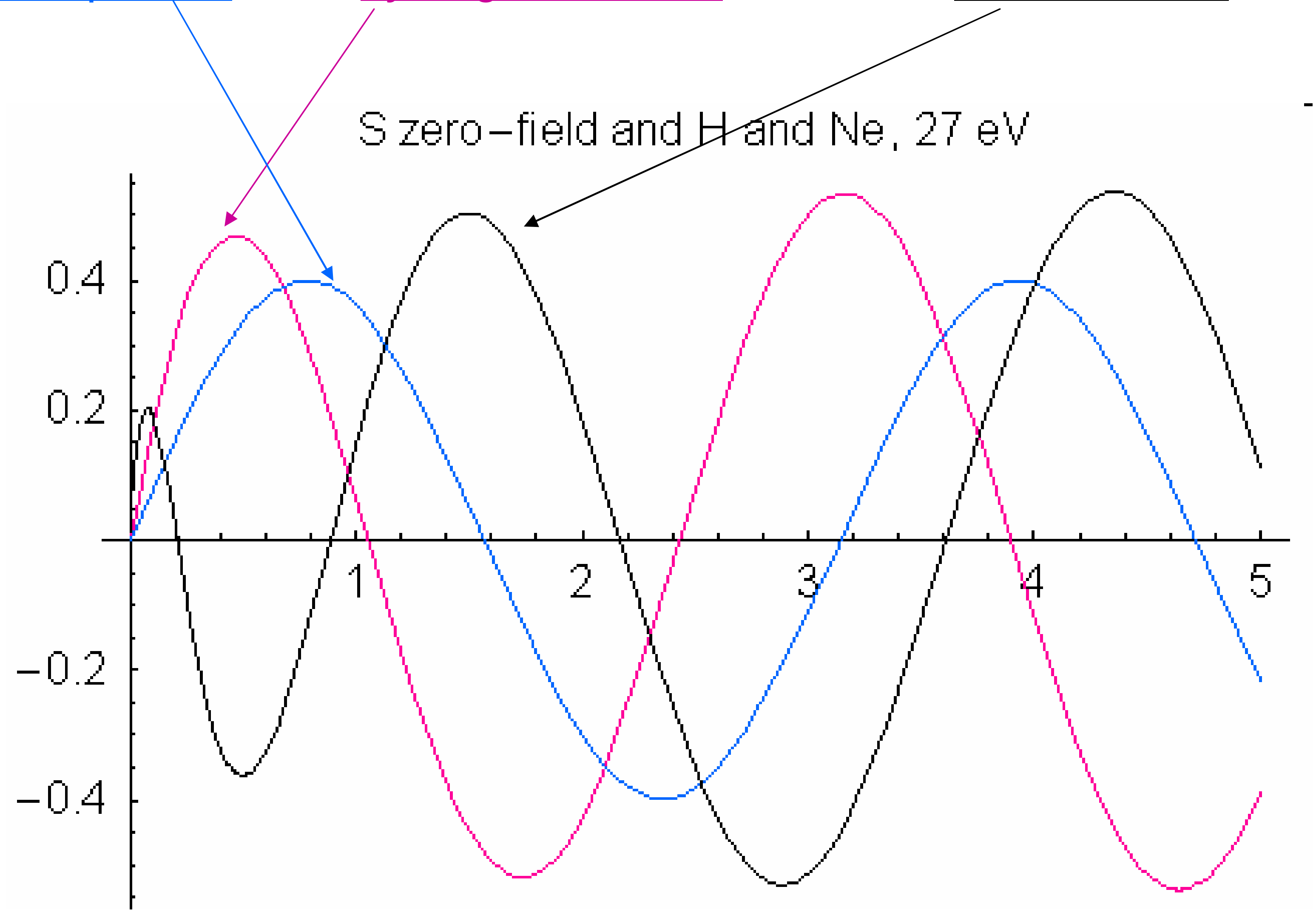

Coulomb continuum effects in molecular interference

G L Yudin[1,2], S Chelkowski[1] and A D Bandrauk[1]

J. Phys. B: At. Mol. Opt. Phys. 39 (2006) L17–L24

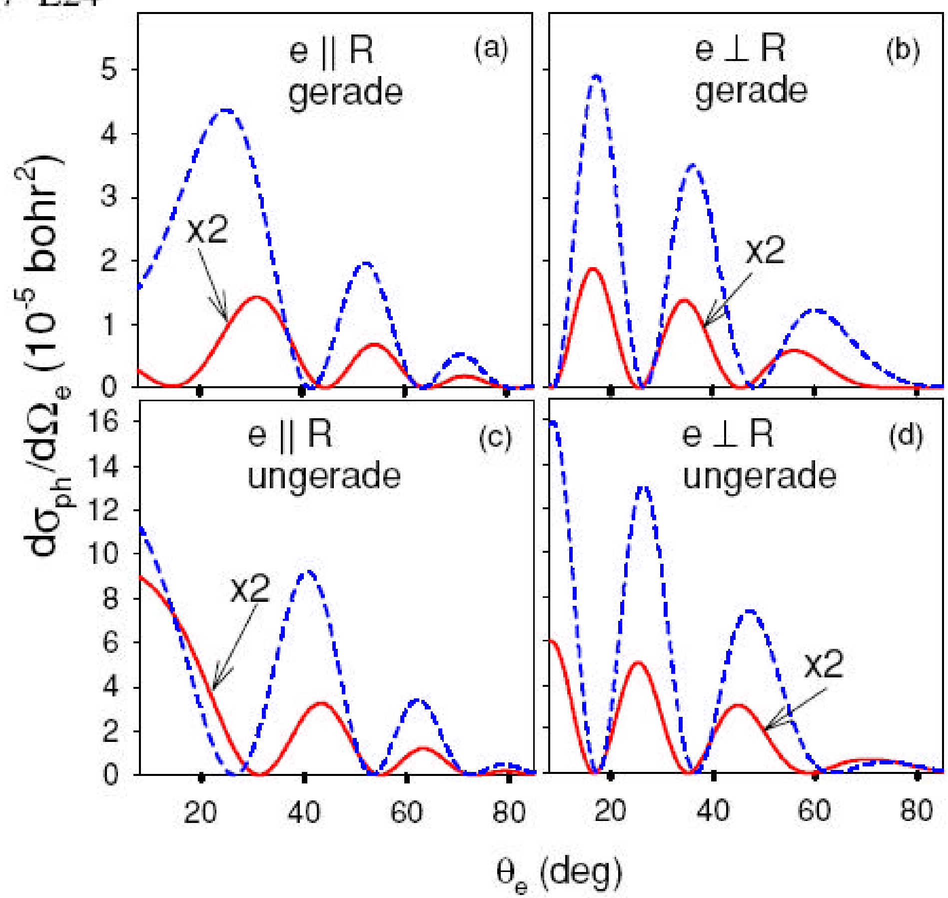

Figure 2. Angular photoelectron distributions at the same parameters as in figure 1. Figures (a, b) and (c, d) correspond to the initial $\sigma_g 2s$ and $\sigma_u 2s$ states of the H_2^+ molecular ion and interference factors χ_+ and χ_-.

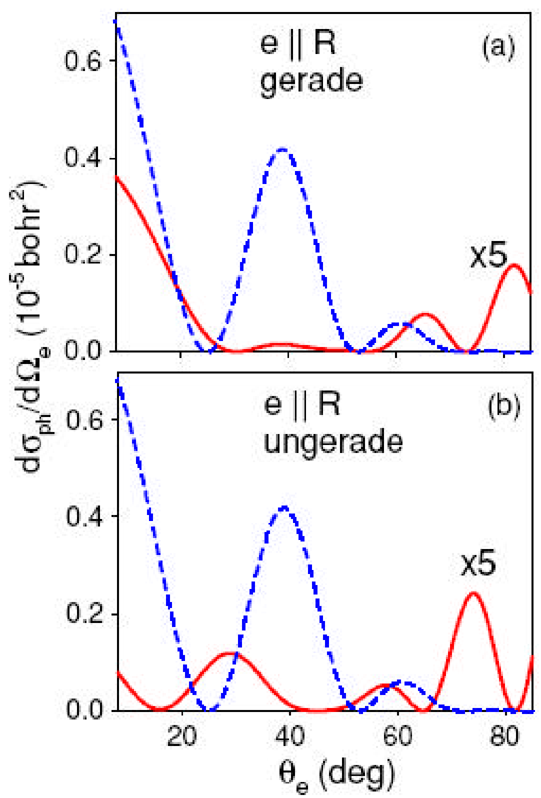

Figure 3. Angular photoelectron distributions at the same parameters as in figure 1. Figures (a) and (b) correspond to the initial $\sigma_g 2p_0$ and $\sigma_u 2p_0$ states of the H_2^+ molecular ion and interference factors χ_- and χ_+.

Spectral Distribution of Atomic Oscillator Strengths*

U. FANO†
Department of Physics, University of Chicago, Chicago, Illinois

J. W. COOPER
National Bureau of Standards, Washington, D.C.

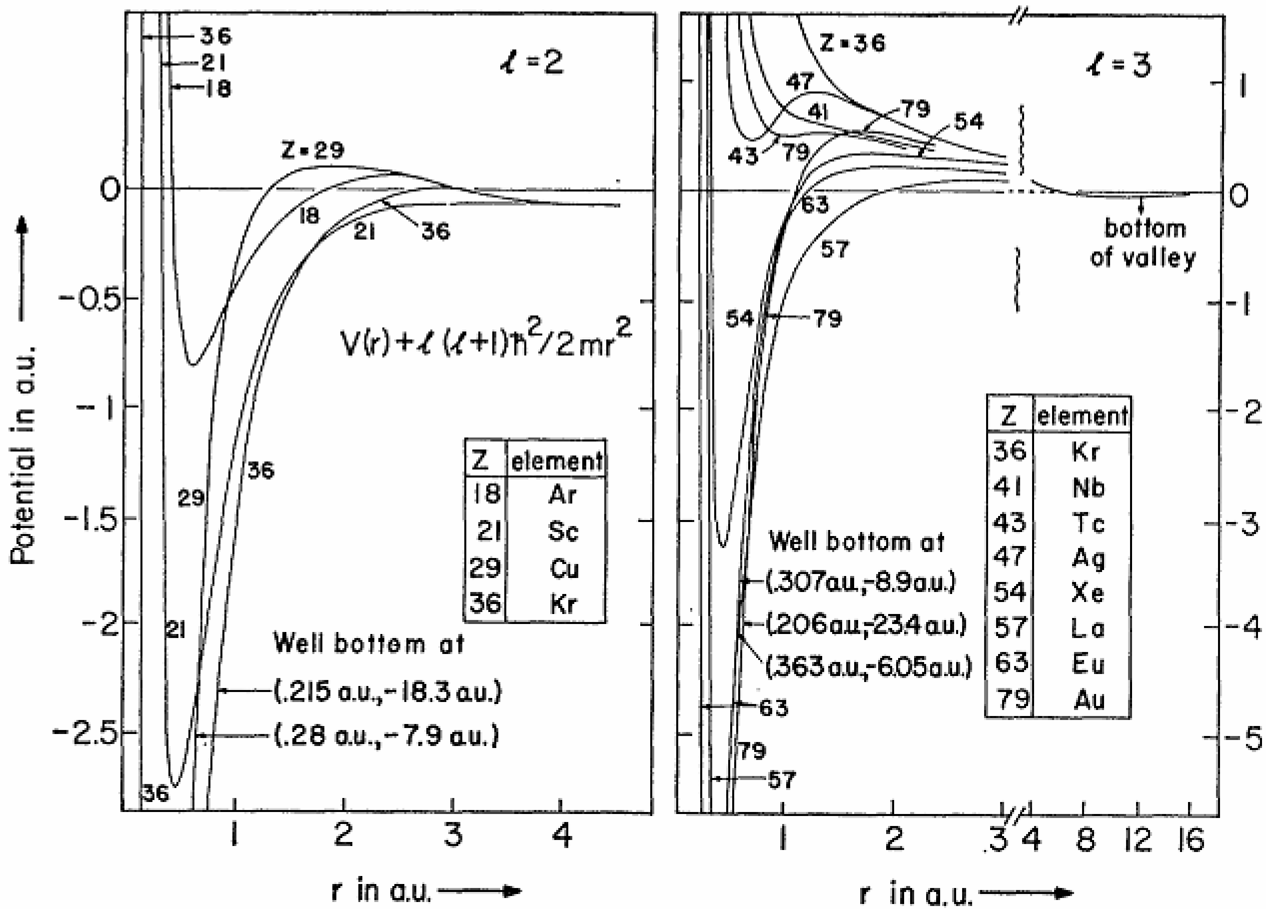

FIG. 17. Sum of electrostatic and centrifugal potentials for electrons with $l=2, 3$ (RF68).

PHYSICAL REVIEW A, VOLUME 61, 020701(R)

Photoionization of atomic iodine and its ions

M. Ya. Amusia,[1,2,*] N. A. Cherepkov,[3] L. V. Chernysheva,[1] and S. T. Manson[4]

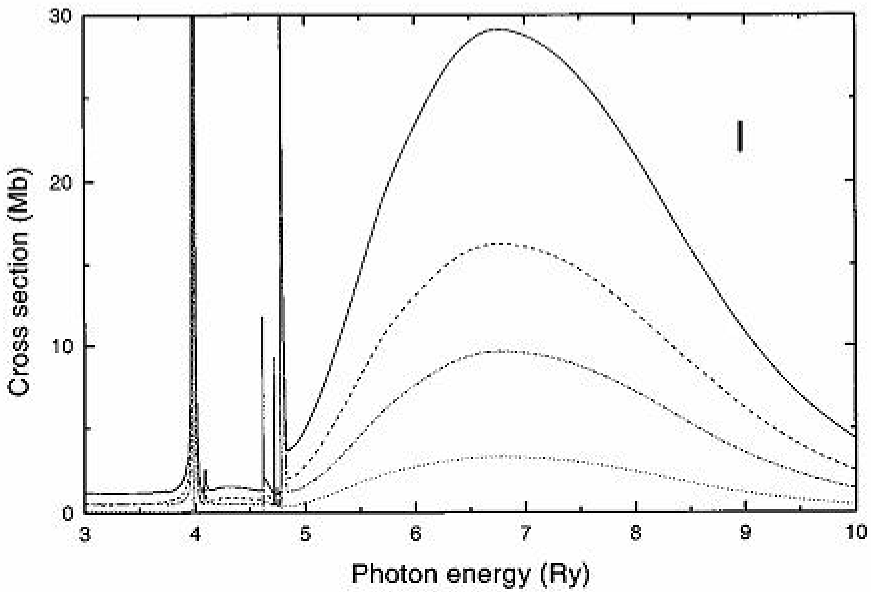

FIG. 2. Calculated total photoabsorption cross section (solid curve) for I in the length formulation in the region of the $4d$ giant resonance, along with the partial cross sections for ^2D (dashed curve), ^2P (dot-dashed curve), and ^2S (dotted curve) final channels, all in length formulation.

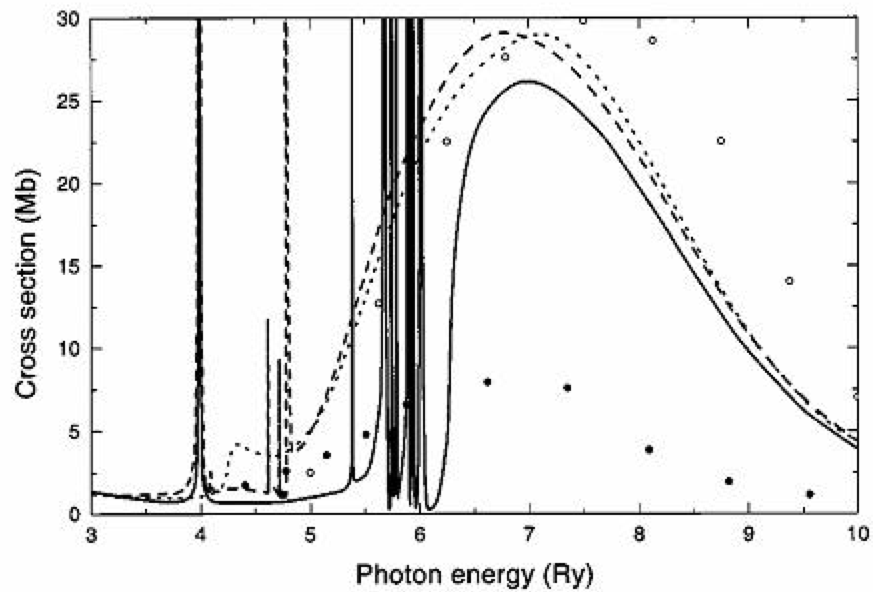

FIG. 4. Comparison of the calculated cross sections for I^- (dotted curve), atomic I (dashed curve), and I^+ (solid curve) in the region of the $4d$ giant resonances along with the experimental points for atomic I [2] (solid dots) and the previous theoretical results for I [4,5] (open dots).

Shape Resonance in 4*d* Inner-Shell Photoionization Spectra of Antimony Clusters

C. Bréchignac, M. Broyer,[a] Ph. Cahuzac, M. de Frutos, P. Labastie,[b] and J.-Ph. Roux
Laboratoire Aimé Cotton, Bâtiment 505, 91405 Orsay CEDEX, France
and Laboratoire pour l'Utilisation du Rayonnetment Electromagnétique, Bâtiment 209, 91405 Orsay CEDEX, France
(Received 31 May 1991)

The photoionization of antimony clusters has been studied in the energy range 20–120 eV, probing the inner-valence 4*d*-*np* transitions as well as the shape resonance 4*d*-εf. When the cluster size is varied the photoionization efficiency presents a quite surprising behavior: For all clusters, except the Sb_{4p} group with $p>1$, the photoionization pattern is similar to that which is known for the bulk. On the other hand, the shape resonance collapses completely for Sb_{4p}. It is further shown that this dramatic change

VOLUME 67, NUMBER 10 PHYSICAL REVIEW LETTERS 2 SEPTEMBER 1991

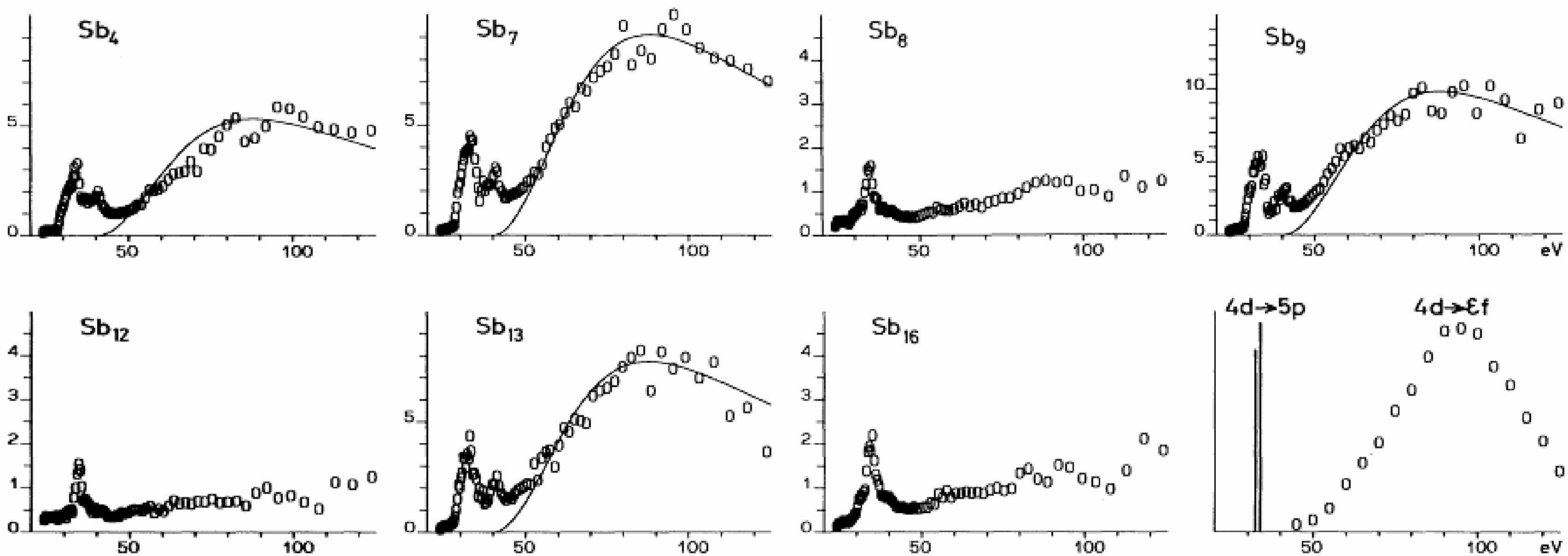

FIG. 1. Photoionization cross section normalized by Eq. (1) for Sb_n with $n=4,7,8,9,12,13,16$ in the 25–120 eV range. The absolute value is in arbitrary units. Solid line is the calculated profile from Ref. [15]; only its intensity is adjusted to fit the data. Also shown is the shape resonance of antimony in GaSb crystal from Ref. [16]. The 4*d* binding energies referred to the Fermi level are represented by vertical bars [15].

Idea: In the rescattering/recombination step the strongest interactions in the problem are the electron-ion and electron-electron interactions, so we propose to treat that physics directly

Background: There have been many approximate treatments of electron-molecule scattering, dating back to the mid-1970s, when the basic phenomena like shape resonances began to succumb to theoretical descriptions (McKoy, Dill and Dehmer, Schneider, Collins, Lucchese, Gianturco, Morrison, Lane, Rescigno, Orel,…)

Most of these methods have used single center partial wave expansions. Tonzani and I decided to develop a 3D finite-element R-matrix method that would not require a single-center partial wave expansion to converge the K-shell orbitals centered on each nucleus.

THE JOURNAL OF CHEMICAL PHYSICS **122**, 014111 (2005)

Electron–molecule scattering calculations in a 3D finite element *R*-matrix approach

Stefano Tonzani
JILA, University of Colorado, Boulder, Colorado 80309-0440

Chris H. Greene

Simplest tesselation scheme: parallelepipeds in spherical coordinates

$$u(\xi_1,\xi_2,\xi_3)=\sum_{i,j,k,l,m,n}\psi_i^l(\xi_1)\psi_j^m(\xi_2)\psi_k^n(\xi_3)C_{\text{node}}^{(lmn)}$$

$$a_{k,p}=x_{k,p,i+1}-x_{k,p,i},$$

$$x_{k,p}=a_{k,p}\xi_k+x_{k,p,i},$$

$$\Gamma_{ij}=\int\left[\sum_{k=1}^{3}\frac{F(x_k)}{a_k^2}\frac{\partial u_i}{\partial\xi_k}\frac{\partial u_j}{\partial\xi_k}+2u_i(U-E)u_j\right]$$
$$\times a_r a_\theta a_\phi r^2\sin^2\theta d\xi_1 d\xi_2 d\xi_3,$$

$$\Lambda_{mn}=\int Y_{lm}^*(\theta,\phi)Y_{l'm'}(\theta,\phi)\sin\theta\ d\theta d\phi$$
$$=\delta_{ll'}\delta_{mm'},$$

Local (Hara) exchange→

$$V_{ex}(\mathbf{r})=-\frac{2}{\pi}k_F F(\eta),$$

whereas the Fermi momentum k_F electron that is at the top of the Fe gas) is

$$k_F(\mathbf{r})=(3\pi^2\rho(\mathbf{r}))^{1/3}.$$

The other functions present in Eq.

$$F(\eta)=\frac{1}{2}+\frac{1-\eta^2}{4\eta}\log\left|\frac{1+\eta}{1-\eta}\right|,$$

$$\eta=\frac{k}{k_F},$$

variational principle,

$$b=-\frac{\partial\log(r\Psi_\beta)}{\partial r}=2\frac{\int_V\Psi^*(E-\hat{H}-\hat{L})\Psi dV}{\int_V\Psi^*\delta(r-r_0)\Psi dV},$$

for the logarithmic derivative of the wave function.

a generalized eigenvalue problem for b:

$$\underline{\Gamma}\mathbf{C}=(E-\underline{H}-\underline{L})\mathbf{C}=\underline{\Lambda}\mathbf{C}b, \tag{8}$$

where $\underline{\Lambda}$ is the overlap of the basis functions calculated on the surface of the R-matrix box and $\hat{L}$ is the Bloch operator, defined as

$$\hat{L}=\frac{1}{2}\delta(r-r_0)\frac{\partial}{\partial r}r$$

$$\Omega\mathbf{C}_o=(\underline{\Gamma}_{oo}-\underline{\Gamma}_{oc}\underline{\Gamma}_{cc}^{-1}\underline{\Gamma}_{co})\mathbf{C}_o=\underline{\Lambda}_{oo}\mathbf{C}_o b$$

in the open functions subspace, in addition iliary system of equations,

$$\underline{\Gamma}_{cc}\mathbf{C}_c=-\underline{\Gamma}_{co}\mathbf{C}_o,$$

Sample grid choice for e-CO_2

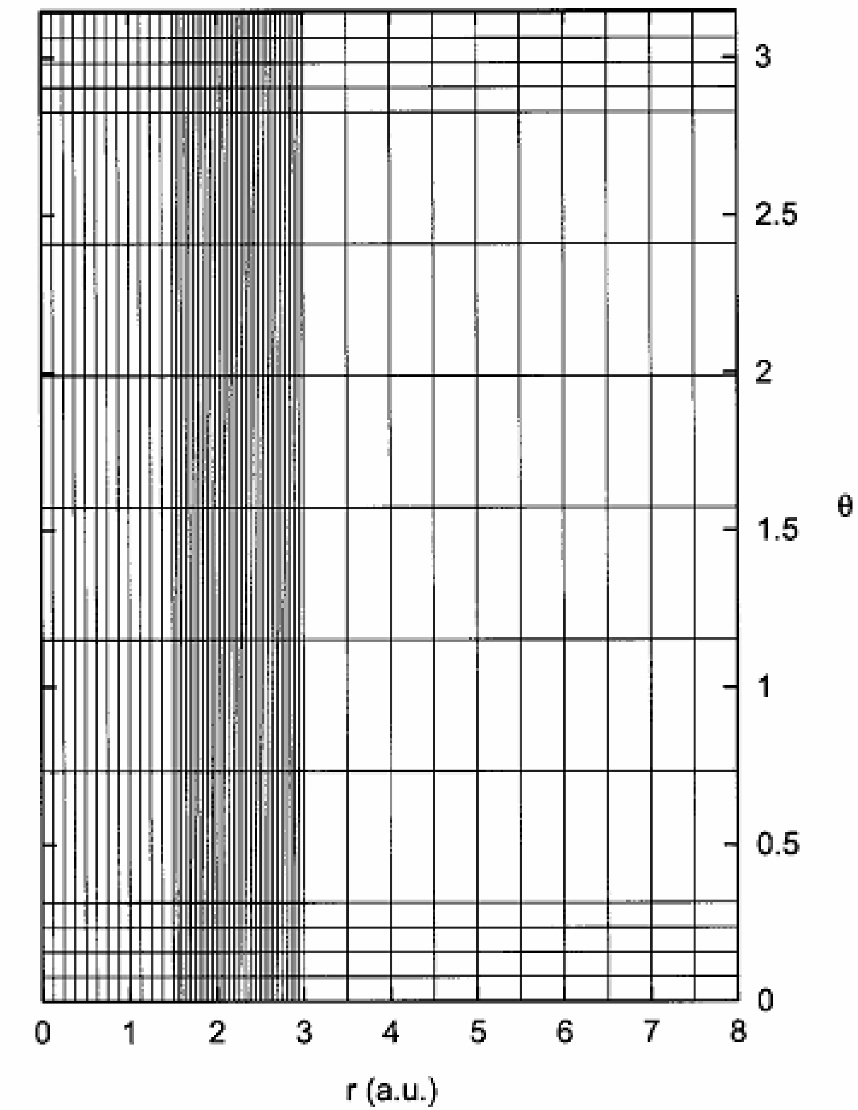

FIG. 1. From this two-dimensional cut in the radius r and the polar angle θ of the finite element grid (for a CO_2 target), it is possible to notice the finer mesh near the oxygen nuclei localized at $r = 2.19$ a.u. and $\theta = 0$ and π, respectively, while the carbon is located at the center of the grid.

Sample test calculation for e-CO2

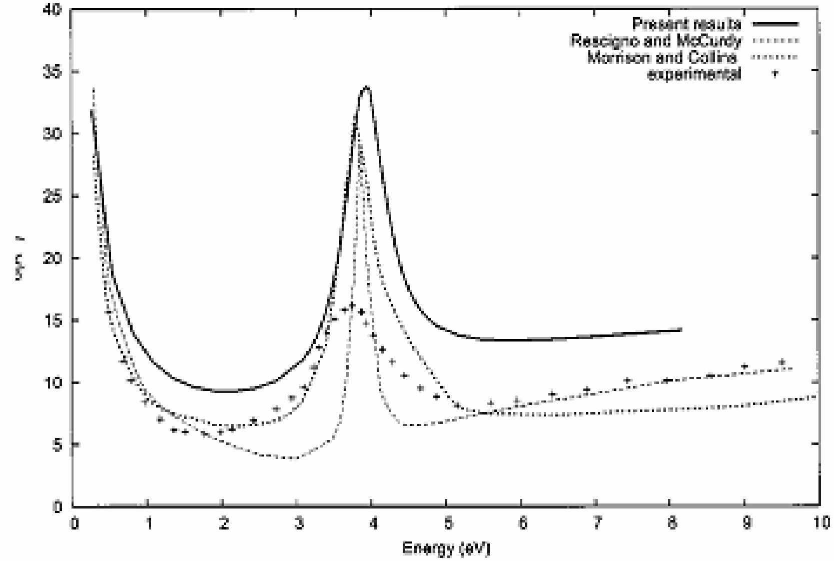

G. 4. Total elastic cross section for scattering of electrons from CO_2 . The esent results are compared with previous theory from Rescigno *et al.* (Ref.) and Morrison and Lane (Ref. 6), whereas the experimental results are ose of Szmytkowski (Ref. 45).

Sample test calculation for e-N_2

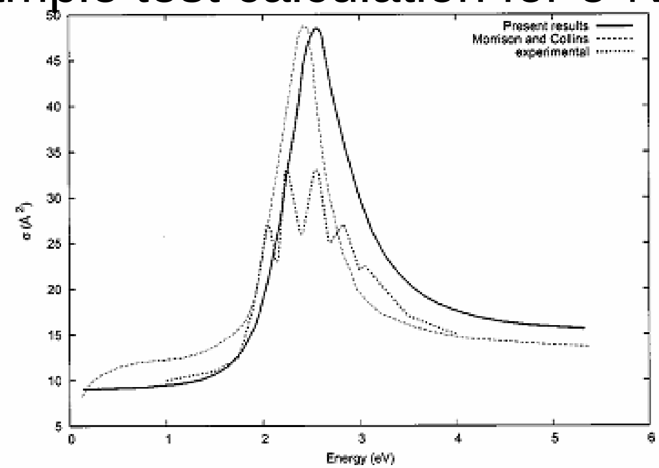

FIG. 3. Total elastic cross section for electron-N_2 scattering, compared to the theoretical results of Morrison and Collins (Ref. 4) and experimental cross section of Kennerly (Ref. 44).

Typical sparsity pattern for Hamiltonian and related matrices

THE JOURNAL OF CHEMICAL PHYSICS **124**, 054312 (2006)

Low-energy electron scattering from DNA and RNA bases: Shape resonances and radiation damage

Stefano Tonzani[a]
JILA and Department of Chemistry, University of Colorado, Boulder, Colorado 80309-0440
Chris H. Greene

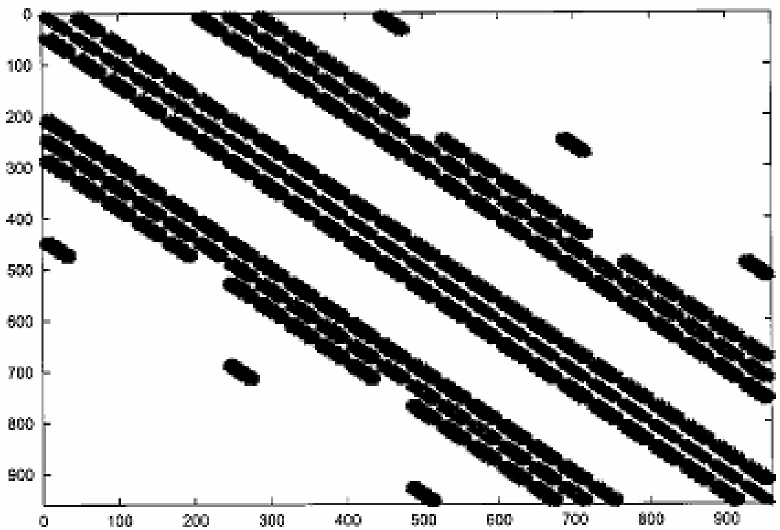

FIG. 7. Structure of the finite element matrix Γ for a small test case of dimension 900. It is possible to notice the great sparsity of the matrix, which increases with the dimension of the matrix.

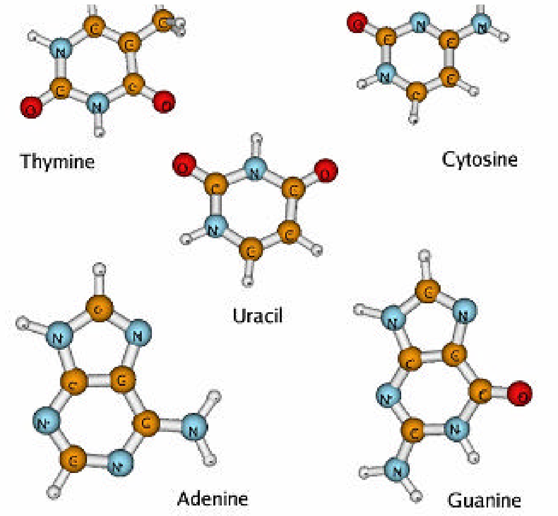

e-adenine scattering

e-guanine scattering

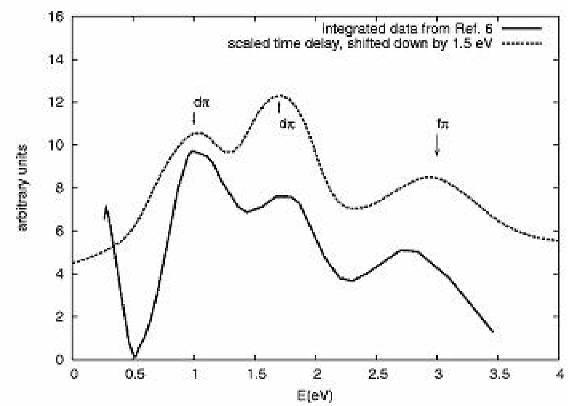

FIG. 6. Comparison with the experimental data of Aflatooni *et al.* (Ref. 6) for adenine. The arrows indicate the resonance positions from the present work, while labels show the dominant partial wave of resonance. The time-delay curve is shifted downward by 1.5 eV to have the position of the first resonance coincide with the experimental data.

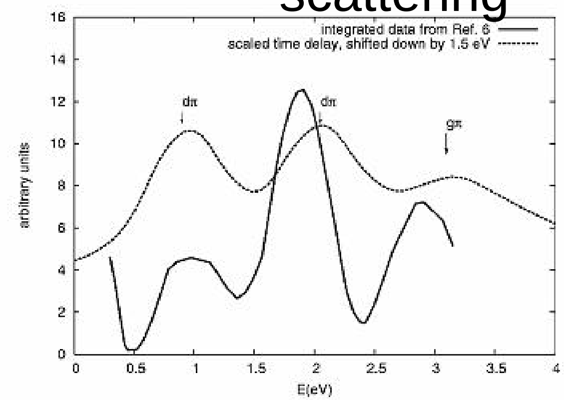

FIG. 7. Comparison with the experimental data of Aflatooni *et al.* (Ref. 6) for guanine. The arrows indicate the resonance positions from the present work, while labels show the dominant partial wave of the resonances. The time-delay curve is shifted downward by 1.5 eV to have the position of the first resonance coincide with the experimental data.

e-scattering wavefunctions - Adenine

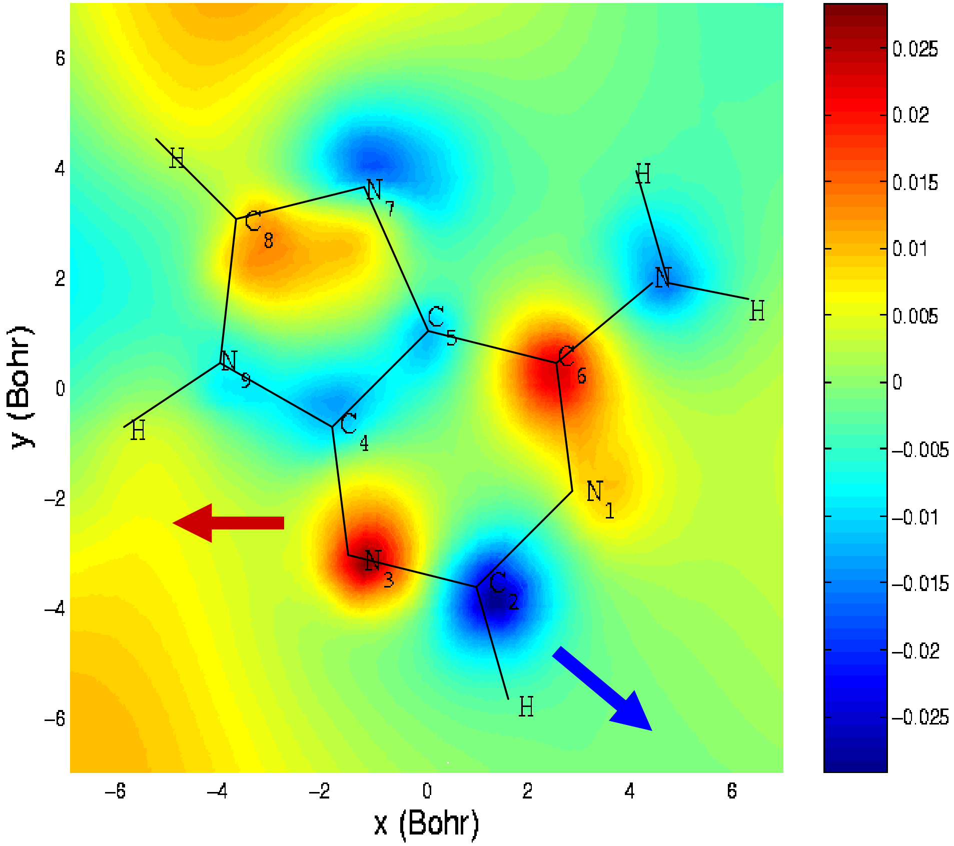

2.2 eV

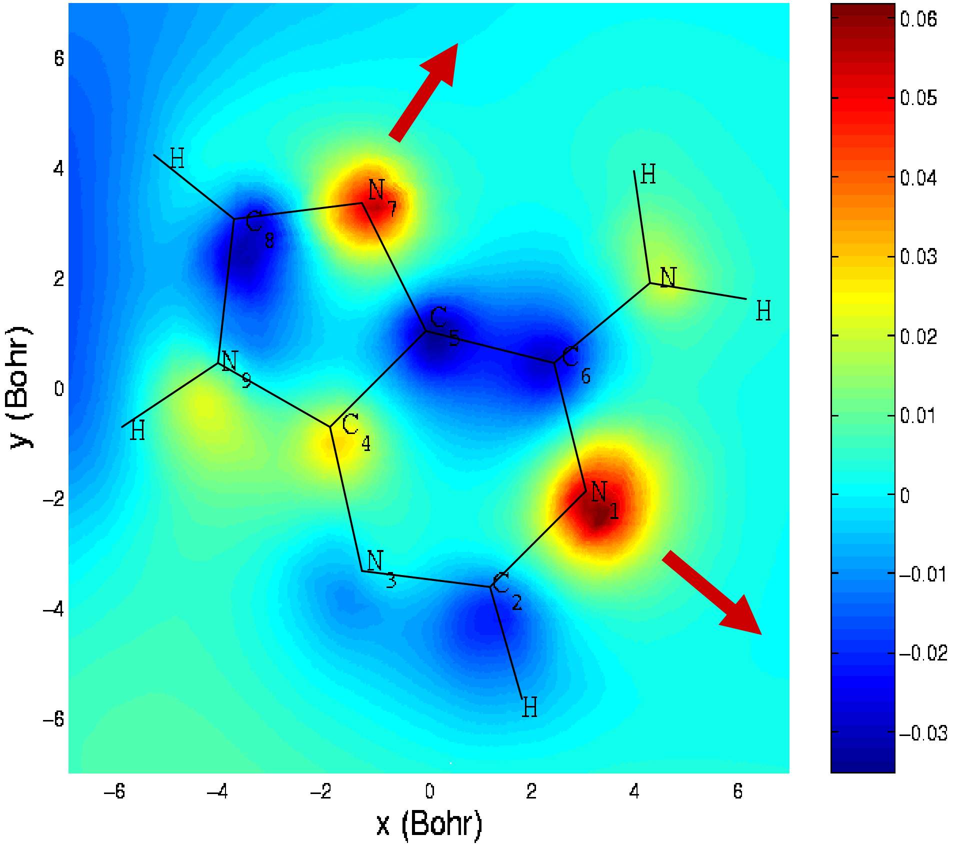

2.6 eV

Shape resonance wavefunctions are similar to 1st and 2nd virtual orbitals

(Tonzani and CHG, 2006 J. Chem. Phys.)

Testing the plane wave approximation against results using realistic molecular scattering wavefunctions, or using a simple Coulomb wave

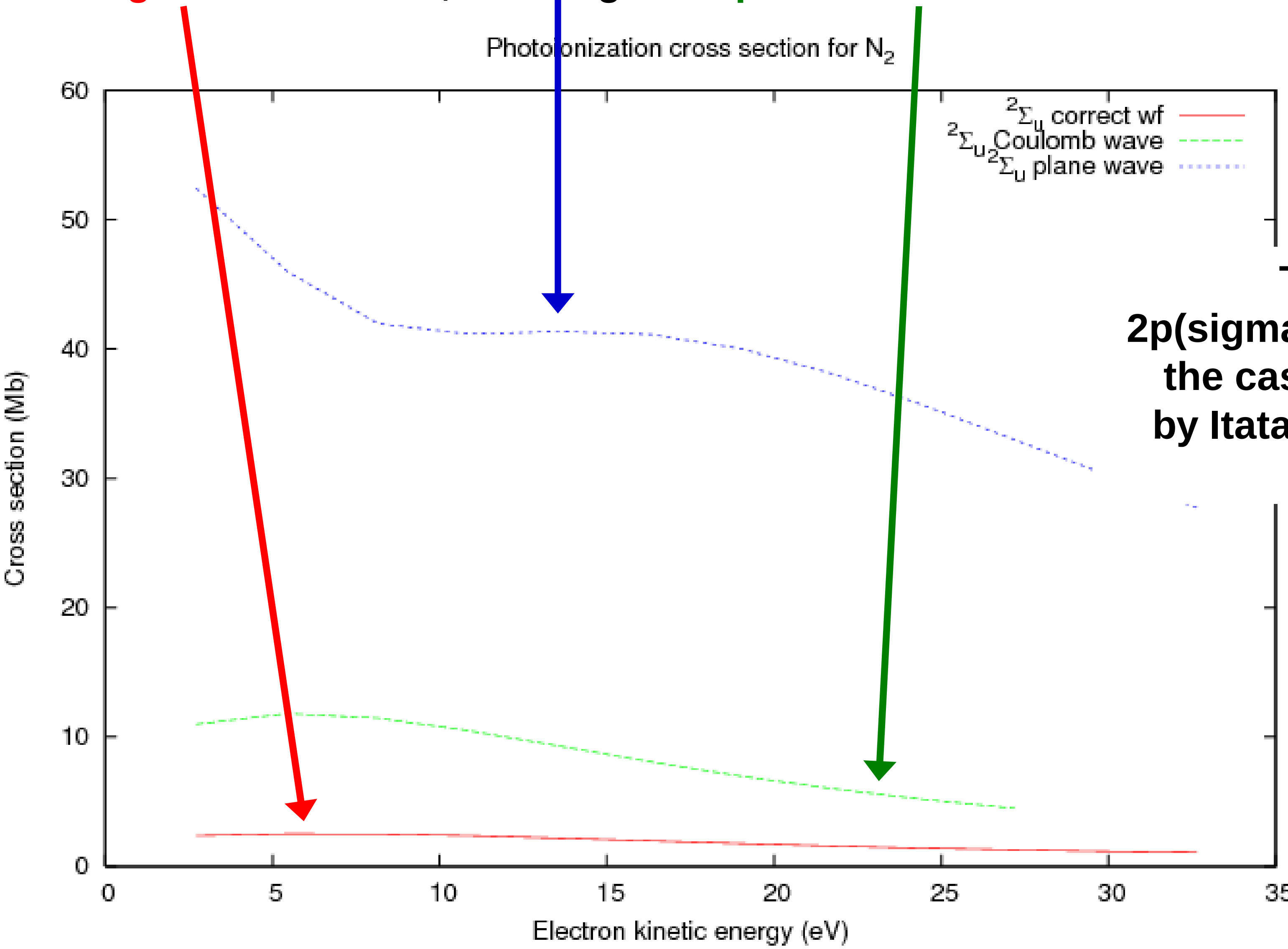

This is the 2p(sigma$_u$) orbital, the case studied by Itatani, Nature (2004)

Note that the *magnitude* of the cross section is predicted incorrectly in the plane wave approximation, by more than an order of magnitude.

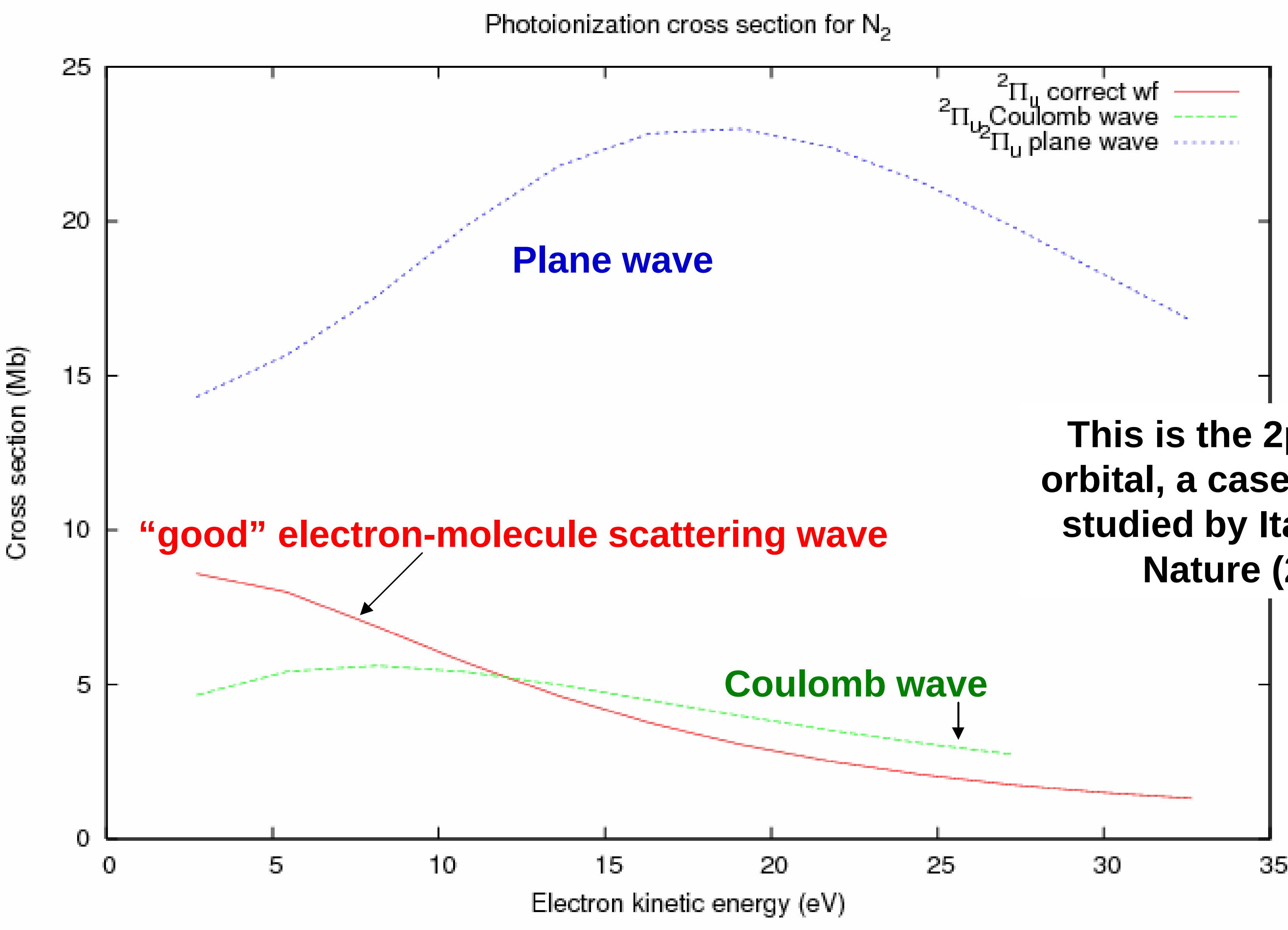

This is the 2p(pi$_u$) orbital, a case NOT studied by Itatani, Nature (2004)

Itatani et al., Nature (2004)

$$I(\omega) \propto \omega^4 |d(\omega)|^2 \qquad \Psi_c = \int a(k) \exp[ik(\omega)x] \mathrm{d}k$$

$$\mathbf{d}(\omega) = a[k(\omega)] \int \psi_g(\mathbf{r})(e\mathbf{r}) \exp[ik(\omega)x] \mathrm{d}\mathbf{r}.$$

Instead,Tonzani, Walters, and CHG propose (unpublished):

A more realistic treatment begins from eigenstates of the

electron scattering from the molecular ion, $h_{mol} u_\varepsilon = \varepsilon u_\varepsilon$:

$$\boxed{\Psi(r,t) = \int d\varepsilon\, u_\varepsilon(r) a_\varepsilon(t) e^{-i\varepsilon t/\hbar} d\varepsilon}$$

where $a_\varepsilon(t)$ ≈time-independent when h_{mol} dominates over h_{laser}

Here is how to carry out the tomography more accurately. Replace the Fourier analysis into plane waves by a decomposition of the rescattering wavepacket in terms of electron-molecule scattering eigenstates:

$$\Psi(\vec{r},t) = \int u_\varepsilon(\vec{r}) a_\varepsilon(t) e^{-i\varepsilon t/\hbar} d\varepsilon$$

where $a_\varepsilon(t)$ ≈time-independent when h_{mol} dominates over h_{laser}

$$d_x(\omega) = a_\varepsilon \int \psi_g^*(\vec{r}) \; ex \; u_\varepsilon(\vec{r}) d^3 r$$

evaluated at $\omega = (\varepsilon - \varepsilon_0)/\hbar$. And now carry out the inverse transform using the orthonormal and complete scattering states:

$$a_\varepsilon \psi_g^*(\vec{r}) \; ex \; = \int u_\varepsilon^*(\vec{r}) d_x[(\varepsilon - \varepsilon_0)/\hbar] d\varepsilon$$

Of course, this requires a realistic scattering wavefunction to be calculated, but this is now fairly routine at the independent-electron level. See, e.g., S. Tonzani, FEM-R-matrix program, submitted to Computer Physics Communications in 2006.

Conclusion from part 2:

For tomographic orbital reconstruction experiments, it is advisable to avoid using the plane wave approximation, because it is probably too inaccurate to be generally useful, below electron energies of at least several hundred eV for light molecules, and probably at least keV for molecules with deeper inner-shell electrons.

However, if good electron-scattering eigenfunctions can be calculated theoretically, including the multiple-center nature of the potential, this concept can be reformulated to describe more quantitatively the nature of the electron-molecule interaction.